International Forum on Aeroelasticity and Structural Dynamics
IFASD 2017
25-28 June 2017 Como, Italy

FREE-FLIGHT NONLINEAR AEROELASTIC SIMULATIONS OF THE X-HALE UAV BY AN EXTENDED MODAL APPROACH

Markus Ritter[1], **Jessica Jones**[2], **Carlos E. S. Cesnik**[3]

[1]DLR - Institute of Aeroelasticity, Bunsenstraße 10, 37073 Göttingen, Germany
markus.ritter@dlr.de

[2]Graduate Research Assistant, Department of Aerospace Engineering
University of Michigan, Ann Arbor, Michigan 48109-2140
jrenejo@umich.edu

[3]Professor, Department of Aerospace Engineering
University of Michigan, Ann Arbor, Michigan 48109-2140
cesnik@umich.edu

Keywords: X-HALE, Very flexible Aircraft, Geometrically Large Deformations, Extended Modal Approach, Nonlinear Flight Dynamics, Unsteady Vortex-Lattice

Abstract: A recently proposed method that extends the classical modal approach captures geometrically nonlinear effects in large structural deflections. The extensions account for nonlinear force displacement relationship by generalized quadratic and cubic stiffness terms and a geometrically nonlinear displacement field by quadratic, cubic, and fourth-order mode components. These extensions make the method particularly suitable for aeroelastic applications involving highly flexible structures and nonlinearities due to nonconservative loads. In this work, the method is enhanced by rigid body degrees of freedom to simulate a maneuvering, very flexible aircraft. Special emphasis is put on the derivation of a set of coupled differential equations of motion in which as few assumptions as possible are made with respect to structural deformations. The use of the mean-axes constraints is explicitely avoided, all inertial and gyroscopic coupling terms between rigid body and elastic motion are included. The setup of the aeroelastic framework based on an unsteady vortex-lattice method in the time doamin is presented in detail. University of Michigan's X-HALE UAV is the test case of this work. The results of dynamic maneuvers including tail input scenarios and gust encounters are presented and compared with results from UM/NAST.

1 INTRODUCTION

Some classes of aircraft are characterized by highly flexible airframes exhibiting pronounced structural deflections in steady and maneuvering flight. High altitude, long endurance (HALE) type of aircraft as well as modern, high performance sailplanes are prominent examples. Design criteria such as reduction of the induced drag almost inevitably lead to wings of high slenderness and aspect ratio. Analyzing and designing highly flexible aircraft puts great demands on the methods and tools employed. Multidisciplinary analysis taking into account aerodynamics, flight mechanics, and structural dynamics is indispensable where nonlinearities due to large rigid body and structural deflections are inherent in each of these disciplines and must be taken into account from the beginning. For the structural part, only few methods exist so far for the

calculation of general aircraft structures undergoing large deformations. Commercial Finite Element solver are mostly limited to clamped structures in their nonlinear solution capabilities. On the other hand, sophisticated methods incorporating nonlinear rigid body and elastic motions have been developed for beam type structural models only. A recently developed method (the extended modal approach) is aiming to fill this gap by extension of the classical modal approach to account for its major limitations [1–3]. Nonlinear force-displacement relations and a geometrically nonlinear displacement field are accounted for as well as a load dependent stiffness function, similar to the geometric stiffness matrix used in nonlinear finite element analyses. In this work, the method is further extended by rigid body degrees of freedom in a nonlinear fashion to enable the simulation of the free-flying elastic aircraft. The differential equations of motion are derived using Lagrange's equations in quasi- and modal coordinates. Inertial and gyroscopic coupling terms between rigid body and elastic motions are taken into account and enable the use of shape functions for the calculation of structural deformations with clamped boundary condition, which are required by the extended modal approach. In combination with an unsteady vortex-lattice solver, an aeroelastic framework is presented for trim and maneuver simulations of highly flexible aircraft in the time domain.

The test case of this work is the *X-HALE* UAV from the Active Aeroelasticity and Structures Research Laboratory from University of Michigan. The goal of this UAV project is the development of a low cost test bed to obtain and provide nonlinear aeroelastic data [4]. The concept and setup of the X-HALE platform is depicted in Fig. 1. Pronounced nonlinear aeroelastic and flight

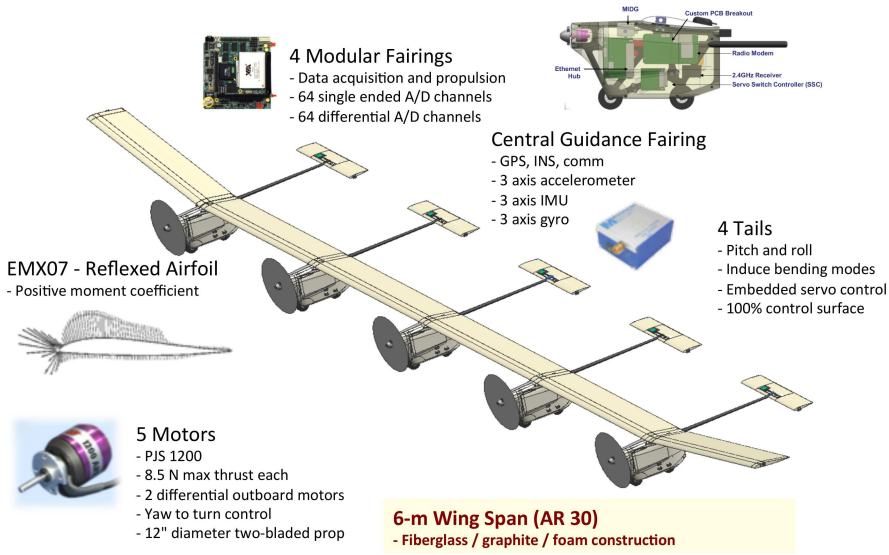

Figure 1: Concept of the X-HALE UAV developed by University of Michigan [4].

dynamics interactions make this aircraft a very challenging test case for numerical simulations. Classical aeroelastic and flight dynamic analysis of elastic aircraft based on coupling of linear aerodynamic methods such as DLM, with linear structural dynamics methods, are completely losing their validity for such an application.

2 THEORY OF THE ENHANCED MODAL APPROACH

The derivation of the enhanced modal approach is given in detail in Ref. [1], the final governing equations are presented in the following. Compared to the classical modal approach, the proposed method is based on a nonlinear force-displacement relationship by quadratic and cubic stiffness terms, as given in the following nonlinear governing equation in pseudo-generalized

coordinates:

$$ {}^{p}G_1^i \, q_i \; + \; {}^{p}G_2^{ij} \, q_i q_j \; + \; {}^{p}G_3^{ijk} \, q_i q_j q_k = Q^p \;\; (p = 1, \ldots, m) \tag{1} $$

Where the ${}^{p}G_n$ tensors denote the generalized stiffnesses and $\boldsymbol{q}$ the vector of generalized coordinates. The stiffness tensors G_n are determined by polynomial fitting or numerical differentiation [1].

The second extension is the reconstruction of a geometrically nonlinear displacement field based on higher-order mode components (here up to fourth order). Usually, the structure's eigenvectors realize the linear transformation from generalized to physical coordinates. For the proposed method this linear relationship is extended, the mode shape ${}^{p}\boldsymbol{\Phi}$ includes components of higher-order and becomes a function of generalized coordinates:

$$ {}^{p}\boldsymbol{\Phi} = {}^{p}\boldsymbol{\Phi}_0 + {}^{p}\boldsymbol{\Phi}_1^i \, q_i + {}^{p}\boldsymbol{\Phi}_2^{ij} \, q_i q_j + {}^{p}\boldsymbol{\Phi}_3^{ijk} \, q_i q_j q_k \tag{2} $$

The term ${}^{p}\boldsymbol{\Phi}_0$ can be seen as the equivalent of the structure's normal modes.

Considering Eq.(1), the forcing term of the structure's governing equation, the generalized force Q^p, is normally calculated by the product of the transposed eigenvector matrix and the forces on the structure's nodes, $\boldsymbol{f}$. Here, the quadratic mode components ${}^{p}\boldsymbol{\Phi}_1^i$ extend the generalized forces to yield a dependency of Q^p on the amplitude of deformation:

$$ Q^p = {}^{p}\boldsymbol{\Phi}_0{}^{T} \boldsymbol{f} + {}^{p}\boldsymbol{\Phi}_1^{i\,T} \boldsymbol{f} \, q_i \tag{3} $$

Combining Eq.(1) and (3) yields:

$$ ({}^{p}G_1^i - {}^{p}\boldsymbol{\Phi}_1^{i\,T} \boldsymbol{f} \,) \, q_i + {}^{p}G_2^{ij} \, q_i \, q_j + {}^{p}G_3^{ijk} \, q_i \, q_j \, q_k = {}^{p}\boldsymbol{\Phi}_0{}^{T} \boldsymbol{f} \tag{4} $$

Eq.(4) is the static governing equation of the enhanced modal approach. Compared to the classical modal approach, the ${}^{p}G_1^i$ term is amended by the product of the transpose of the quadratic mode component matrix and the force field. This additional stiffness parameter is of importance especially in aeroelastic applications [1, 2]. Subsequent to the solution of the governing equation for the generalized coordinates $\boldsymbol{q}$, the nodal deformation field in cartesian coordinates is approximated by the higher order mode components:

$$ \mathbf{u}(\boldsymbol{q}) = {}^{p}\boldsymbol{\Phi}_0 \, q_p + {}^{p}\boldsymbol{\Phi}_1^i \, q_p q_i + {}^{p}\boldsymbol{\Phi}_2^{ij} \, q_p q_i q_j + {}^{p}\boldsymbol{\Phi}_3^{ijk} \, q_p q_i q_j q_k \tag{5} $$

3 THEORETICAL DEVELOPMENT OF THE FLIGHT DYNAMIC EQUATIONS OF MOTION

This section describes the derivation of the flight dynamic equations of motion for the free flying elastic aircraft where elastic structural deformations are calculated by means of the extended modal approach. The goal is to obtain a set of equations in which rigid body and elastic degrees of freedom (the independent variables) are coupled by inertial and gyroscopic forces. This coupling is retained deliberately because of two reasons. First, any attempt to decouple rigid body and elastic motions is based on a particular choice for the location of the body fixed reference frame. Using the aircraft's instantaneous center of gravity leads to the mean-axes constraints which are met by structural mode shapes with free-free boundary conditions (unclamped model). This approach is based on various assumptions, such as small structural deformations which is excluded in this work a priori. Second, the higher-order stiffness and mode tensors are

determined by a series of nonlinear structural simulations. Such simulations can be done with a clamped structural model only.

The derivation is based on Lagrange's equations of the second kind in quasi- and modal coordinates and loosely based on the work from Buttrill and Meirovitch [5, 6]. In contrast to Buttrill's derivation the inertial coupling terms between rigid body and elastic DOFs are kept. A lumped mass model of the structure with discrete masses is used.

3.1 Definition of kinematic relationships

Two coordinate systems are used for the definition of the kinematics, a geodetic, earth-fixed system and a body fixed frame, depicted in Fig. 2. The geodetic system is considered as inertial

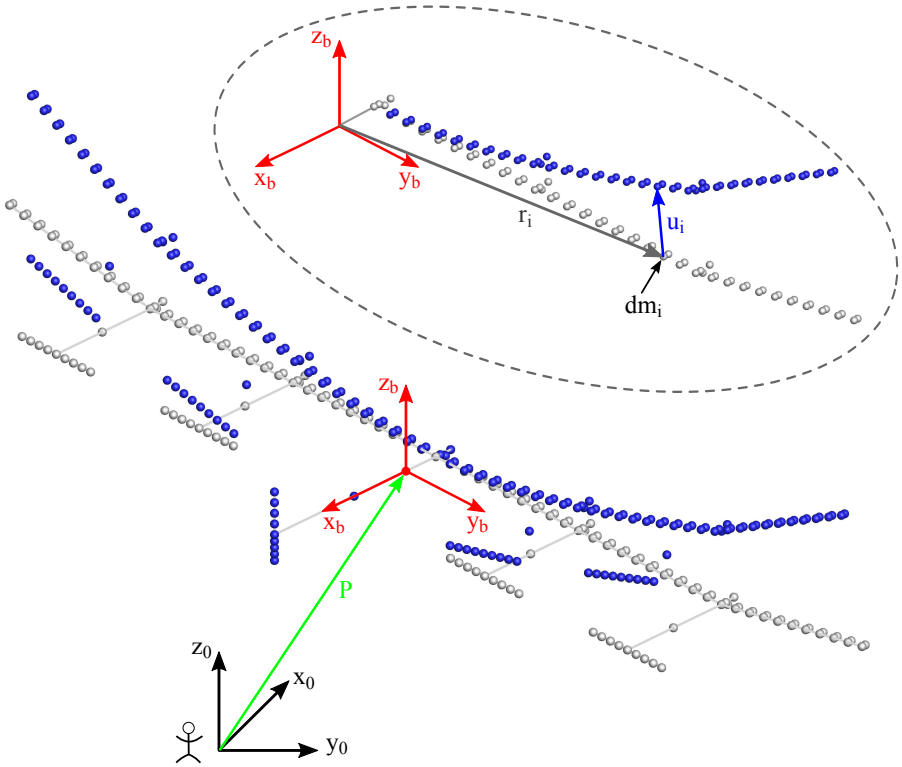

Figure 2: Inertial (geodetic) and body fixed coordinate systems with indices 0 and b (body system fixed to the undeformed body). Mass point dm_i in undeformed position, r_i, and displacement due to structural deformation, u_i.

system, its basis vectors are denoted by $\boldsymbol{x}_g$, $\boldsymbol{y}_g$, and $\boldsymbol{z}_g$. In the following, the coordinate system fixed to a material point of the aircraft in its undeformed position is denoted as body fixed frame or body system, with basis vectors defined as $\boldsymbol{x}_b$, $\boldsymbol{y}_b$, and $\boldsymbol{z}_b$. The summation index i refers to a discrete mass dm_i of the lumped mass model, where n denotes the number of mass points. The location of the body frame in the geodetic frame is defined by vector $\boldsymbol{P}$, it is resolved in the body frame. The set of Euler angles is used to define the attitude of the body frame within the geodetic frame [7]:

$$\underline{\boldsymbol{\Phi}} = [\, \Phi \;\; \Theta \;\; \Psi \,]^T \; . \tag{6}$$

Angular rates of the body frame resolved in the body frame are denoted by vector $\boldsymbol{\Omega}_b$:

$$\boldsymbol{\Omega}_b = [\, p \;\; q \;\; r \,]^T \; . \tag{7}$$

The vector $\boldsymbol{R}_i$ denotes the location of a discrete mass point resolved in the inertial frame:

$$\boldsymbol{R}_i = \boldsymbol{P} + \boldsymbol{r}_i + \boldsymbol{u}_i \ , \tag{8}$$

where $\boldsymbol{r}_i$ defines the position of the mass point in the body fixed frame with respect to the undeformed structure, and $\boldsymbol{u}_i$ is the displacement of the mass point due to structural deformation, also resolved in the body fixed frame. The velocity of the mass point, $\dot{\boldsymbol{R}}_i$, is given by the total time derivative of the position vector $\boldsymbol{R}_i$ and will be denoted as $\boldsymbol{V}_i$ in the following:

$$\dot{\boldsymbol{R}}_i = \dot{\boldsymbol{P}} + \boldsymbol{\Omega}_b \times \boldsymbol{P} + \mathring{\boldsymbol{u}}_i + \boldsymbol{\Omega}_b \times (\boldsymbol{r}_i + \boldsymbol{u}_i) = \boldsymbol{V}_i \ . \tag{9}$$

A ring above a variable denotes its time rate of change with respect to the body frame. The term $\dot{\boldsymbol{P}} + \boldsymbol{\Omega}_b \times \boldsymbol{P}$ corresponds to the translational velocity of the body frame resolved in the body frame:

$$\boldsymbol{V}_b = \dot{\boldsymbol{P}} + \boldsymbol{\Omega}_b \times \boldsymbol{P} \ , \tag{10}$$

with the following velocity components along the particular axes:

$$\boldsymbol{V}_b = [\, u \ v \ w \,]^T \ . \tag{11}$$

Transformation of a vector resolved in the geodetic frame into the body fixed frame is done by rotation matrix $\boldsymbol{M}_{bg}$. This matrix is also used to calculate the kinematical relation between the time derivative of the position vector $\boldsymbol{P}$ and the body frame's translational velocity [7]:

$$\boldsymbol{V}_b = \boldsymbol{M}_{bg}\, \dot{\boldsymbol{P}} \ . \tag{12}$$

Calculating the body frame's angular velocity $\boldsymbol{\Omega}_b$ from the time rate of change of the Euler angles requires another transformation matrix denoted by $\boldsymbol{M}_{b\Phi}$ [7]:

$$\boldsymbol{\Omega}_b = \boldsymbol{M}_{b\Phi}\, \underline{\dot{\boldsymbol{\Phi}}} \ . \tag{13}$$

3.2 Kinetic Energy Expression

The kinetic energy of the aircraft is given by the sum of the kinetic energies of its n discrete masses dm_i:

$$T = \frac{1}{2} \left(\sum_{i=1}^{n} \boldsymbol{V}_i^T \boldsymbol{V}_i \, dm_i \right) + \frac{1}{2} \boldsymbol{\Omega}_b^T \sum_{i=1}^{n} \boldsymbol{J}_i \, \boldsymbol{\Omega}_b \ , \tag{14}$$

where the local tensor of inertia of an individual mass point is denoted by $\boldsymbol{J}_i$. The sum of the discrete masses yields the aircraft's total mass, m:

$$m = \sum_{i=1}^{n} dm_i \ . \tag{15}$$

Inserting the velocity defined by Eq.(9) into Eq.(14) results in the following expression for the kinetic energy of the structure [5].

$$
\begin{aligned}
T = & \frac{1}{2}\,\boldsymbol{V}_b^T \boldsymbol{V}_b\, m + \frac{1}{2}\sum_{i=1}^{n} \mathring{\boldsymbol{u}}_i^T \mathring{\boldsymbol{u}}_i\, dm_i \\
& + \frac{1}{2}\,\boldsymbol{\Omega}_b^T \left[\sum_{i=1}^{n} \left[\left(\boldsymbol{r}_i^T \boldsymbol{r}_i\right) \boldsymbol{I} - \boldsymbol{r}_i \boldsymbol{r}_i^T\right] dm_i\right] \boldsymbol{\Omega}_b \\
& + \frac{1}{2}\,\boldsymbol{\Omega}_b^T \left[\sum_{i=1}^{n} \left[\left(\boldsymbol{u}_i^T \boldsymbol{r}_i + \boldsymbol{r}_i^T \boldsymbol{u}_i\right) \boldsymbol{I} - \boldsymbol{u}_i \boldsymbol{r}_i^T - \boldsymbol{r}_i \boldsymbol{u}_i^T\right] dm_i\right] \boldsymbol{\Omega}_b \\
& + \frac{1}{2}\,\boldsymbol{\Omega}_b^T \left[\sum_{i=1}^{n} \left[\left(\boldsymbol{u}_i^T \boldsymbol{u}_i\right) \boldsymbol{I} - \boldsymbol{u}_i \boldsymbol{u}_i^T\right] dm_i\right] \boldsymbol{\Omega}_b \\
& + \boldsymbol{\Omega}_b^T \left[\sum_{i=1}^{n} \left(\boldsymbol{u}_i \times \mathring{\boldsymbol{u}}_i\right) dm_i\right] + \boldsymbol{V}_b^T \left[\boldsymbol{\Omega}_b \times \left(\sum_{i=1}^{n} \left(\boldsymbol{r}_i + \boldsymbol{u}_i\right) dm_i\right)\right] \\
& + \boldsymbol{V}_b^T \left[\sum_{i=1}^{n} \mathring{\boldsymbol{u}}_i dm_i\right] + \boldsymbol{\Omega}_b^T \left[\sum_{i=1}^{n} \left(\boldsymbol{r}_i \times \mathring{\boldsymbol{u}}_i\right) dm_i\right] + \frac{1}{2}\,\boldsymbol{\Omega}_b^T \sum_{i=1}^{n} \boldsymbol{J}_i\, \boldsymbol{\Omega}_b \ .
\end{aligned}
\tag{16}
$$

The nodal displacement $\boldsymbol{u}_i$ of a mass point dm_i due to structural deformation is calculated by the modal approach. For simplicity, only the linear ${}^{p}\boldsymbol{\Phi}_0$ components are used for now. However, the quadratic mode components are considered for the reconstruction of the physical displacement field, cf. Eq.(5) in the final equations of motion for the aircraft. Hence, $\boldsymbol{u}_i$ is calculated as:

$$
\boldsymbol{u}_i = {}^{p}\boldsymbol{\Phi}_0^i\, q_p \ \ (p = 1, \ldots, m) \ . \tag{17}
$$

With the corresponding time derivative given as:

$$
\dot{\boldsymbol{u}}_i = {}^{p}\boldsymbol{\Phi}_0^i\, \dot{q}_p \ . \tag{18}
$$

Equation (18) is inserted into Eq.(16) to express nodal deformations as function of generalized coordinates. The resulting terms of Eq.(16) are discussed now.

$$
\frac{1}{2}\sum_{i=1}^{n} \mathring{\boldsymbol{u}}_i^T\, \mathring{\boldsymbol{u}}_i\, dm_i = \frac{1}{2}\, M_{pk}\, \dot{q}_p\, \dot{q}_k \tag{19}
$$

denotes the modal kinetic energy of the elastic deformations where M_{pk} is the generalized mass matrix. Definitions for the tensor of inertia and its derivatives are introduced in the following to simplify the equations of motion [5]. The tensor of inertia of the undeformed aircraft with the local inertia contributions is given by the following expression:

$$
\boldsymbol{J} \equiv \sum_{i=1}^{n} \left[\left(\boldsymbol{r}_i^T \boldsymbol{r}_i\right) \boldsymbol{I} - \boldsymbol{r}_i \boldsymbol{r}_i^T\right] dm_i + \sum_{i=1}^{n} \boldsymbol{J}_i \ . \tag{20}
$$

The first-order effect of deformation on the inertia tensor is considered by tensor $\Delta\boldsymbol{J}$:

$$
\sum_{i=1}^{n} \left[\left(\boldsymbol{u}_i^T \boldsymbol{r}_i + \boldsymbol{r}_i^T \boldsymbol{u}_i\right) \boldsymbol{I} - \boldsymbol{u}_i \boldsymbol{r}_i^T - \boldsymbol{r}_i \boldsymbol{u}_i^T\right] dm_i = \underbrace{\sum_{i=1}^{n} \left[\left(2\boldsymbol{r}_i^T\, {}^{p}\boldsymbol{\Phi}_0^i\right) \boldsymbol{I} - {}^{p}\boldsymbol{\Phi}_0^i \boldsymbol{r}_i^T - \boldsymbol{r}_i {}^{p}\boldsymbol{\Phi}_0^{i\,T}\right] dm_i}_{\Delta \boldsymbol{J}_p}\, q_p \ . \tag{21}
$$

Second-order effect of deformation on the inertia tensor is considered by tensor $\boldsymbol{B}$:

$$\sum_{i=1}^{n}\left[\left(\boldsymbol{u}_i^T\boldsymbol{u}_i\right)\boldsymbol{I}-\boldsymbol{u}_i\boldsymbol{u}_i^T\right]dm_i=\underbrace{\sum_{i=1}^{n}\left[\left({}^{p}\boldsymbol{\Phi}_0^{i\,T}\,{}^{k}\boldsymbol{\Phi}_0^{i}\right)\boldsymbol{I}-{}^{p}\boldsymbol{\Phi}_0^{i}\,{}^{k}\boldsymbol{\Phi}_0^{i\,T}\right]dm_i}_{\boldsymbol{B}_{pk}}\,q_pq_k\ . \tag{22}$$

The following definition is introduced:

$$\Delta^2\boldsymbol{J}_{pk}\equiv\boldsymbol{B}_{pk}+\boldsymbol{B}_{kp}\ . \tag{23}$$

Second-order momentum coupling between elastic modes and angular momentum occurs through the following cross product of modes p and k, denoted by tensor $\boldsymbol{h}$ [5]:

$$\sum_{i=1}^{n}\left(\boldsymbol{u}_i\times\mathring{\boldsymbol{u}}_i\right)dm_i=\underbrace{\sum_{i=1}^{n}\left({}^{p}\boldsymbol{\Phi}_0^{i}\times{}^{k}\boldsymbol{\Phi}_0^{i}\right)dm_i}_{\boldsymbol{h}_{pk}}\,q_p\dot{q}_k\,. \tag{24}$$

If the origin of the body fixed frame is located at the center of gravity of the undeformed structure, the seventh term of Eq.(16) will be identical zero. This removes inertial coupling between the translational and rotational angular momentum. The location of the origin of the body fixed frame with respect to the undeformed aircraft structure is not restricted here and can be chosen according to practical needs, but a location in the plane of symmetry of the aircraft seems favorable. The eighth, ninth, and tenth term of Eq.(16) can be set to zero only if the so-called *mean-axis* conditions are employed. These conditions can be approximated if the eigenvectors of an unrestrained structure are used in Eq.(17) [5]. If the eigenvectors of a clamped structure are to be used for the calculation of elastic deformations, coupling between elastic and translational and angular momentum occurs which is considered by the following contributions to the kinetic energy in Eq.(16):

$$\boldsymbol{V}_b^T\left[\boldsymbol{\Omega}_b\times\left(\sum_{i=1}^{n}\boldsymbol{u}_i\,dm_i\right)\right]=\boldsymbol{V}_b^T\left[\boldsymbol{\Omega}_b\times\left(\left[\sum_{i=1}^{n}{}^{p}\boldsymbol{\Phi}_0^{i}\,dm_i\right]q_p\right)\right] \tag{25}$$

$$\boldsymbol{V}_b^T\left[\sum_{i=1}^{n}\mathring{\boldsymbol{u}}_i\,dm_i\right]=\boldsymbol{V}_b^T\left[\left[\sum_{i=1}^{n}{}^{p}\boldsymbol{\Phi}_0^{i}\,dm_i\right]\dot{q}_p\right] \tag{26}$$

$$\boldsymbol{\Omega}_b^T\left[\sum_{i=1}^{n}\left(\boldsymbol{r}_i\times\mathring{\boldsymbol{u}}_i\right)\,dm_i\right]=\boldsymbol{\Omega}_b^T\left[\left[\sum_{i=1}^{n}\left(\boldsymbol{r}_i\times{}^{p}\boldsymbol{\Phi}_0^{i}\right)dm_i\right]\dot{q}_p\right] \tag{27}$$

Where the first expression describes the coupling between linear and angular momentum. The following definitions are introduced to avoid lengthy expressions in the following derivations.

$$\overline{\boldsymbol{rm}}\equiv\sum_{i=1}^{n}\boldsymbol{r}_i\,dm_i \tag{28a}$$

$${}^{p}\overline{\boldsymbol{\Phi m}}\equiv\sum_{i=1}^{n}{}^{p}\boldsymbol{\Phi}_0^{i}\,dm_i \tag{28b}$$

$${}^{p}\overline{\boldsymbol{r\Phi m}}\equiv\sum_{i=1}^{n}\left(\boldsymbol{r}_i\times{}^{p}\boldsymbol{\Phi}_0^{i}\right)dm_i \tag{28c}$$

3.3 Potential Energy Expression

The potential energy of the system is the sum of gravity and strain energy:

$$U = U_g + U_s \ . \tag{29}$$

Similar as for the kinetic energy and for simplicity, no higher order mode components are taken into account for the strain energy function. Using only the linear mode component ${}^p\boldsymbol{\Phi}_0^i$ for the calculation of structural deformations in the potential energy expression yields:

$$U = -\sum_{i=1}^{n} \left(\boldsymbol{P} + \boldsymbol{r}_i + {}^p\boldsymbol{\Phi}_0^i \, q_p\right)^T \left(\boldsymbol{M}_{bg}\, \boldsymbol{g}\right) \, dm_i + \frac{1}{2} \left({}^pG_1^i \, q_p q_i + {}^pG_2^{ij} \, q_p q_i q_j \ + \ {}^pG_3^{ijk} \, q_p q_i q_j q_k\right), \tag{30}$$

where the gravity vector, resolved in the geodetic frame, is denoted as $\boldsymbol{g} = [\,0\,0\ -g\,]^T$.

3.4 Definition of the generalized forces

The nonconservative generalized forces and moments for translational and rotational momentum as well as for the structural work are denoted as $\boldsymbol{Q}_t$, $\boldsymbol{Q}_r$, and Q^p, respectively. It is assumed that the generalized forces of the translational and angular momentum are composed of aerodynamic and propulsive (thrust) forces and moments only:

$$\boldsymbol{Q}_t = \boldsymbol{R}^A + \boldsymbol{F} \tag{31}$$

$$\boldsymbol{Q}_r = \boldsymbol{Q}^A + \boldsymbol{Q}^F \tag{32}$$

Here, $\boldsymbol{R}^A$ denotes the resulting aerodynamic forces with respect to the axes of the body fixed frame, and $\boldsymbol{F}$ denotes the resulting propulsive forces, also resolved in the body fixed system. Accordingly, $\boldsymbol{Q}^A$ are the resulting aerodynamic moments, and $\boldsymbol{Q}^F$ denotes the propulsive moments. The generalized forces of the structural governing equation are calculated by Eq.(3).

3.5 Lagrange's equations of the second kind in quasi- and modal coordinates

The derivation of the governing differential equations of motion for the free-flying elastic arcraft is based on Lagrange's equations of the second kind in quasi- and modal coordinates, given by Meirovitch [6, 8]. With the Lagrange variable L defined as the difference of kinetic and potential energy, Lagrange's equations for the system are then written as:

Linear momentum in quasi-coordinates:

$$\left.\frac{d}{dt}\right|_b \frac{\partial L}{\partial \boldsymbol{V}_b} + \boldsymbol{\Omega}_b \times \left(\frac{\partial L}{\partial \boldsymbol{V}_b}\right) - \boldsymbol{M}_{bg} \frac{\partial L}{\partial \boldsymbol{P}} = \boldsymbol{Q}_t \tag{33}$$

Rotational momentum in quasi coordinates:

$$\left.\frac{d}{dt}\right|_b \frac{\partial L}{\partial \boldsymbol{\Omega}_b} + \boldsymbol{V}_b \times \left(\frac{\partial L}{\partial \boldsymbol{V}_b}\right) + \boldsymbol{\Omega}_b \times \left(\frac{\partial L}{\partial \boldsymbol{\Omega}_b}\right) - \left(\boldsymbol{M}_{b\Phi}^T\right)^{-1} \frac{\partial L}{\partial \boldsymbol{\Theta}} = \boldsymbol{Q}_r \tag{34}$$

Elastic deformation in modal coordinates:

$$\left.\frac{d}{dt}\right|_b \frac{\partial L}{\partial \dot{q}_p} - \frac{\partial L}{\partial q_p} = Q^p \tag{35}$$

Using the expressions for the kinetic and potential energy defined above, and taking the partial derivatives yields the inertially coupled equations of motion.

The linear momentum equation of motion is then given as:

$$\begin{aligned}&\mathring{\boldsymbol{V}}_b\, m + \mathring{\boldsymbol{\Omega}}_b \times \left[\overline{\boldsymbol{rm}} + {}^p\overline{\boldsymbol{\Phi m}}\, q_p\right] + {}^p\overline{\boldsymbol{\Phi m}}\, \ddot{q}_p + \\ &\boldsymbol{\Omega}_b \times \left[\boldsymbol{V}_b\, m + \boldsymbol{\Omega}_b \times \left[\overline{\boldsymbol{rm}} + {}^p\overline{\boldsymbol{\Phi m}}\, q_p\right] + 2\,{}^p\overline{\boldsymbol{\Phi m}}\, \dot{q}_p\right] - (\boldsymbol{M}_{bg}\boldsymbol{g})\, m = \boldsymbol{Q}_t \end{aligned} \tag{36}$$

The rotational momentum equation of motion is given as:

$$\begin{aligned}&\overline{\boldsymbol{J}}\mathring{\boldsymbol{\Omega}}_b + \mathring{\overline{\boldsymbol{J}}}\boldsymbol{\Omega}_b + \boldsymbol{h}_{pk}\dot{q}_p\dot{q}_k + \boldsymbol{h}_{pk}q_p\ddot{q}_k - \mathring{\boldsymbol{V}}_b \times \left[\overline{\boldsymbol{rm}} + {}^p\overline{\boldsymbol{\Phi m}}\, q_p\right] + {}^p\overline{\boldsymbol{r\Phi m}}\, \ddot{q}_p \\ &+ \boldsymbol{V}_b \times \left[\boldsymbol{\Omega}_b \times \left[\overline{\boldsymbol{rm}} + {}^p\overline{\boldsymbol{\Phi m}}\, q_p\right]\right] \\ &+ \boldsymbol{\Omega}_b \times \left[[\boldsymbol{J}]\,\boldsymbol{\Omega}_b + \boldsymbol{h}_{pk}q_p\dot{q}_k - \boldsymbol{V}_b \times \left[\overline{\boldsymbol{rm}} + {}^p\overline{\boldsymbol{\Phi m}}\, q_p\right] + {}^p\overline{\boldsymbol{r\Phi m}}\, \dot{q}_p\right] = \boldsymbol{Q}_r\ , \end{aligned} \tag{37}$$

where the following definitions have been used [5]

$$\overline{\boldsymbol{J}} \equiv \boldsymbol{J} + \Delta\boldsymbol{J}_p q_p + \frac{1}{2}\Delta^2\boldsymbol{J}_{pk}q_p q_k \tag{38}$$

$$\mathring{\overline{\boldsymbol{J}}} \equiv \Delta\boldsymbol{J}_p\dot{q}_p + \Delta^2\boldsymbol{J}_{pk}q_p\dot{q}_k \tag{39}$$

The governing equation of the elastic deformation for mode p is given as:

$$\begin{aligned}&M_{pk}\,\ddot{q}_k + \mathring{\boldsymbol{V}}_b^T\,{}^p\overline{\boldsymbol{\Phi m}} + \mathring{\boldsymbol{\Omega}}_b^T\left[{}^p\overline{\boldsymbol{r\Phi m}} - \boldsymbol{h}_{pk}q_k\right] - \boldsymbol{V}_b^T\left[\boldsymbol{\Omega}_b \times {}^p\overline{\boldsymbol{\Phi m}}\right] - 2\,\boldsymbol{\Omega}_b{}^T\,\boldsymbol{h}_{pk}\dot{q}_k \\ &- \frac{1}{2}\boldsymbol{\Omega}_b^T\left[\Delta\boldsymbol{J}_p + \Delta^2\boldsymbol{J}_{pk}q_k\right]\boldsymbol{\Omega}_b + {}^pG_1^k\,q_k + {}^pG_2^{ki}\,q_k\,q_i + {}^pG_3^{kij}\,q_k\,q_i\,q_j + {}^p\overline{\boldsymbol{\Phi m}}^T\,(\boldsymbol{M}_{bg}\boldsymbol{g}) = Q^p \end{aligned} \tag{40}$$

As can be seen from these equations, the coupling between the three equations of motion not only occurs by means of the aerodynamic forces applied to the aircraft, but also inertially by the terms defined in Eq.(28). In most aeroelastic applications, these terms are implicitly set to zero by the use of free-free mode shapes of an unrestrained vehicle. However, they are kept in this work due to the higher order mode components used for the reconstruction of the physical displacement field, which are obtained for clamped structures only. Structural damping is omitted here, but can be considered in the equation of the elastic deformations.

4 THE AEROELASTIC FRAMEWORK

This section describes the aeroelastic framework which is based on a steady and unsteady VL solver for the calculation of the aerodynamic forces. The unsteady solution sequence coupled with unsteady aerodynamic forces in time domain is shown in Fig. 3 at a glance. Initialization of the aerodynamic model and the setup of the structural model is done in a pre-processing step.

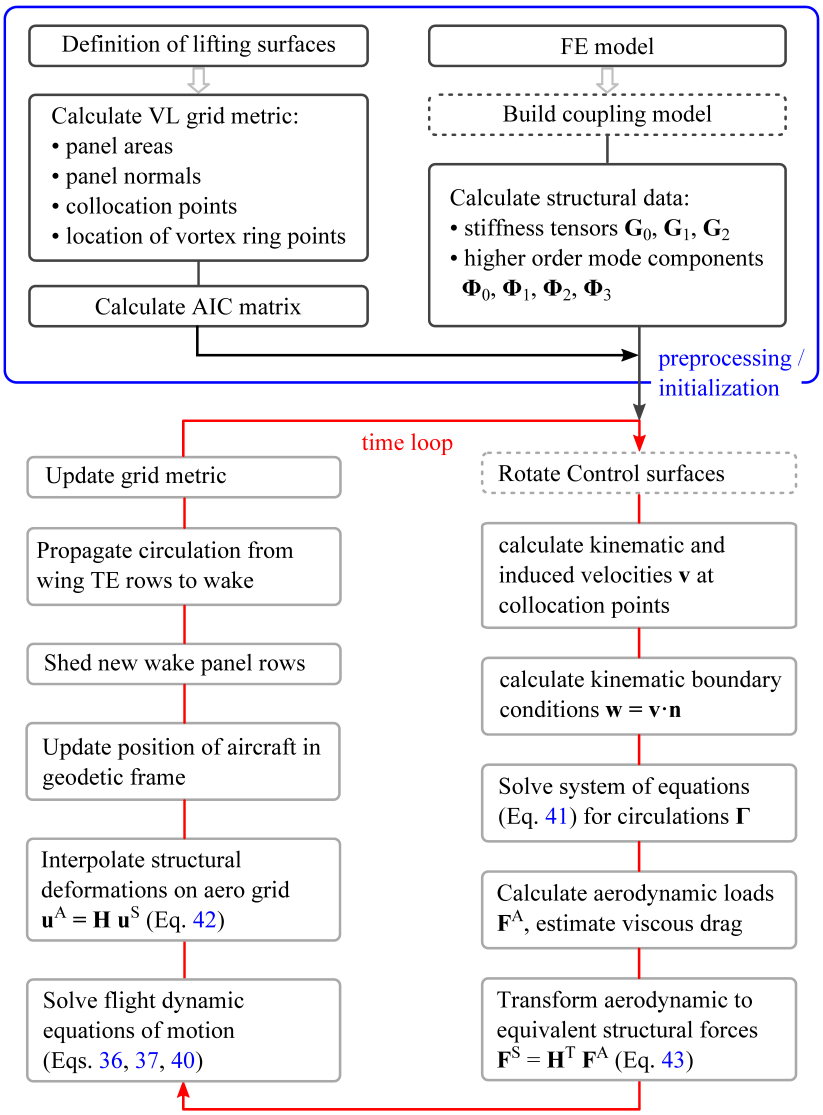

Figure 3: Solution sequence for the flight dynamic simulations with aerodynamic, structural, and data transfer part.

4.1 The Vortex-Lattice Aerodynamic Model

Although several aerodynamic methods for geometrically nonlinear simulations with large deformations are presented in literature, three main reasons support the choice of a VLM for this work:

- An almost unlimited deformation of the structure is possible. Aerodynamic panels can undergo large translations and rotation. This is one of the major advantages of the VLM compared to the *doublet-lattice method* (DLM), which is valid for small out-of plane displacements of lifting surfaces only [9].
- Comparatively fast computing time, even in unsteady mode. Though slower as e.g. the 2D strip theory, the method is much cheaper than solving the unsteady Euler or Navier-Stokes equations using a CFD finite-volume approach.
- High accuracy. Compared to 2D theories, 3D effects (e.g. at the wingtip) are taken into account from the outset. This aspect becomes important especially for highly flexible structures. Furthermore, induced drag is taken into account and viscous drag can be estimated and added easily.

The implementation is based on vortex rings (in contrast to the horseshoe vortex approach) such that unsteady aerodynamic forces can be calculated in discrete time steps by a wake shedding procedure [10]. A linear relation of the kinematic boundary conditions $\boldsymbol{w}$ (downwash) to the circulations $\boldsymbol{\Gamma}$ of each aerodynamic panel is the basis for the VL method:

$$\boldsymbol{AIC} \cdot \boldsymbol{\Gamma} = \boldsymbol{w} \tag{41}$$

The *aerodynamic influence coefficients* matrix $\boldsymbol{AIC}$ relates the velocity that is induced at certain (control) points in the flow domain to the circulation of all elementary solutions. The right hand side $\boldsymbol{w}$ includes the non-penetration condition (zero flow velocity in normal direction) at solid walls and the Kutta condition. Once the circulation $\boldsymbol{\Gamma}$ is determined, the dependent variables, such as aerodynamic loads, pressures, and velocity components can be calculated as function of the circulation. After each time step, the metric of the aerodynamic grid is calculated, including updates of e.g. the panel areas and the normal vectors. To this end, translations and rotations of aerodynamic panels due to structural deformations are always taken into account and no linearization or assumption is made in this regard.

Induced drag can be calculated based on the velocities induced by the trailing segments of the bound and the wake vortex rings onto the bound vortex rings [10]. These velocities are added to the onflow velocity at each panel and tilt the resulting aerodynamic force vector. Viscous forces, such as drag, are not part of a potential method's solution but a simple approach for consideration is to estimate them based on local flow and geometric properties and to add them to the aerodynamic forces. Therefore, drag polars are generated using XFOIL for a set of Reynolds numbers and angles of attack with the airfoil considered. For each row of panels in chordwise direction (strip), the effective angle of attack, onflow velocity, and Reynolds number are calculated based on the flow and geometrical properties of this particular strip. A higher-order method interpolates the drag coefficient from the set of drag polars based on the local strip properties. The viscous forces can then be calculated for each strip using the interpolated drag coeffcients [11].

4.2 Data Transfer between Aerodynamic and Structural Model

Independent discretizations of the structural and the aerodynamic model require methods for the transfer of forces and the interpolation of displacements:

$$\boldsymbol{u}^A = \boldsymbol{H}\, \boldsymbol{u}^S \tag{42}$$

$$\boldsymbol{F}^S = \boldsymbol{H}^T\, \boldsymbol{F}^A \tag{43}$$

The first equation relates the displacement of the structural nodes due to elastic deformation and the corresponding displacements of the points of the aerodynamic grid by a linear mapping with the operator $\boldsymbol{H}$, the *coupling matrix*. The second equation describes the transformation of the aerodynamic loads $\boldsymbol{F}^A$ to structural loads $\boldsymbol{F}^S$. The linear mapping must ensure at least a global conservation of work between the aerodynamic and the structural part and correctly consider rigid-body motions of the structure. In the case of the X-HALE UAV, the structural model is represented by a number of finite beam elements. However, the transfer of moments is not considered by the coupling matrix $\boldsymbol{H}$. To circumvent this problem, a so-called *couplingmodel* is used that extends the one-dimensional beam stucture to a 3D model by adding massless rigid bars (MSC Nastran *RBE2* elements) from the particular structural nodes to the region of the leading and trailing edges. This approach is depicted in Fig. 4.

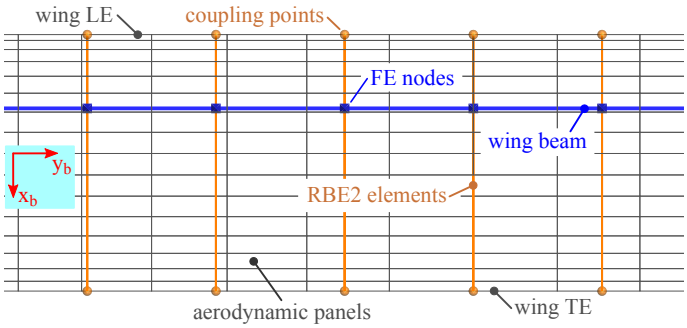

Figure 4: Extension of one-dimensional beam structural model to a 3D model by RBE2-elements.

5 X-HALE TEST CASE: AEROELASTIC MODELS AND UNSTEADY MANEUVER SIMULATIONS

The X-HALE UAV from the University of Michigan is the test case to demonstrate and validate unsteady maneuver simulation results with the method proposed. The X-HALE UAV is a highly flexible, wing-boom-tail type aircraft. It has a six-meter wingspan, to which five booms with horizontal tails are attached, as well as five spines containing motors, batteries, and the instrumentation payload. The mass of the aircraft is 11 kg with flight speeds ranging from 10 to 19 m/s [12]. The wings and the tails are made from fiberglass epoxy composite wrapped around a foam core. The spines and tail booms are made of carbon fiber. The on-board measurement systems consists of an array of sensor to collect data during the flight tests [12]. The UAV serves as a low cost platform to obtain nonlinear aeroelastic data for support and validation of nonlinear aeroelastic codes.

5.1 Nastran FEM of the X-HALE UAV

An MSC Nastran 2D finite element model of the X-HALE was built based on the definition of the model used in UM/NAST. Beam-like components (wings, booms, tails) are modeled by beam-type elements (MSC Nastran *PBEAM* elements), discrete mass elements are added for concentrated masses of structural parts and ballast masses. The structural model is depicted in Fig. 5, where the masses of the discrete mass points are visualized by spheres with aluminum equivalent density. The origin of the body system is located at (0,0,0) with respect to the structural model's coordinate system used in Nastran. It must be mentioned that the structural model is clamped at the origin of the body frame, and thus the wing's flexible beam is clamped at the center. The reason for the clamping is that the determination of the higher-order stiffness and mode components requires a set of nonlinear structural simulations which can only be done with a clamped structure.

5.2 Setup of the VL Aerodynamic Model

The aerodynamic model consists of different lifting surfaces for the wings, the tails, and the spines, as shown in Fig. 6. All elements are lifting surfaces and share wake panels. The UAV is equipped with a *EMX07* reflexed airfoil, and the VL solver uses the camber line calculated from the upper and lower coordinates of the airfoil profile. The incidence of the wing's airfoil is five degrees with respect to the body system's reference frame, as can be seen in Fig. 6. A cosine function is applied for the spacing of the panels on the wing in the spanwise direction to better resolve the wingtip effect, the transition at the dihedral wing elements and at the pods. Any other lifting surfaces are modeled as flat plates.

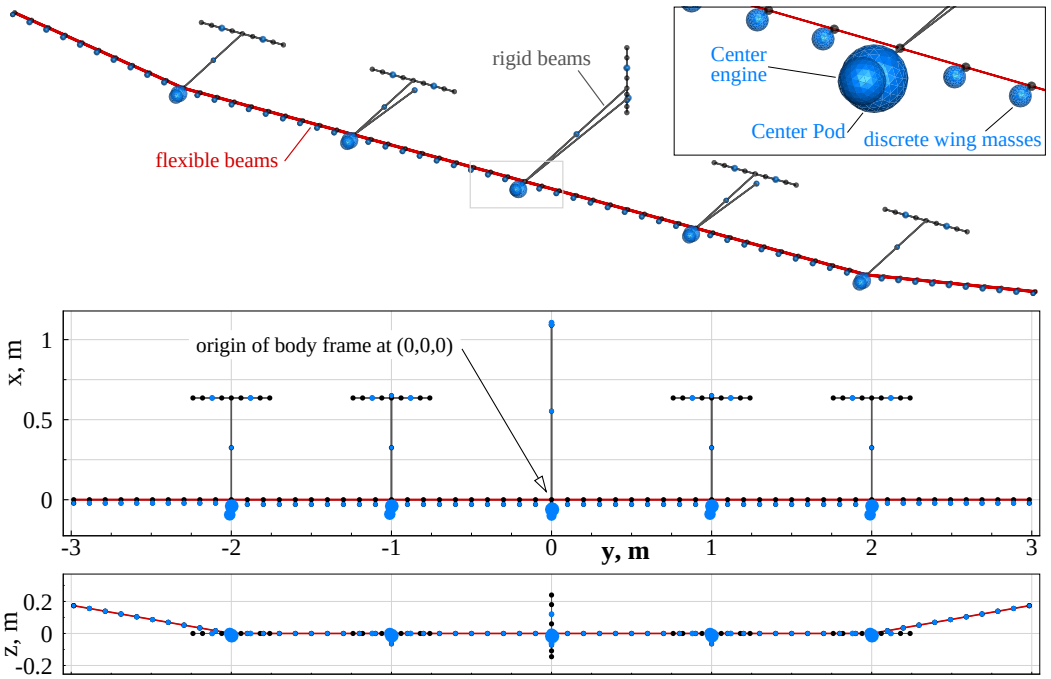

Figure 5: Finite element model of the X-HALE UAV build with flexible and rigid beam finite elements (represented by red and grey lines, respectively). Discrete masses visualized by spheres with aluminum equivalent density.

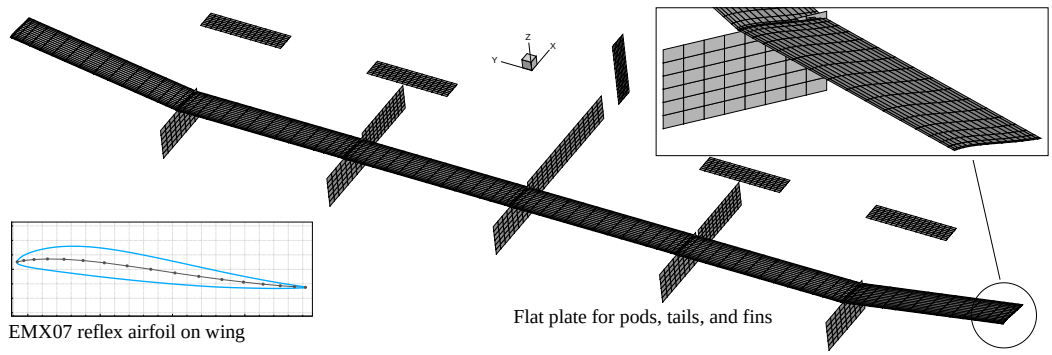

Figure 6: Vortex-lattice grid for the X-HALE composed of several lifting surfaces for the wings, the tails, and the pods.

5.3 Unsteady Maneuvers and Comparison to UM/NAST

Four unsteady maneuvers will be presented in this section. All maneuvers start from a steady horizontal, trimmed flight with a flight velocity of 16 m/s. The trim deflection of the wingtips is approximately 0.16 m. In the first two maneuvers the unsteady excitation of the aircraft is done by a rotation of all four tails simultaneously according to a sinusoidal function with a frequency of 0.25 Hz. The simulation results of the first maneuver (symmetric tail rotation with one degree amplitude) are presented in Fig. 7 in terms of displacement of the wingtip and the pitch angle of the aircraft's body frame as well as the location in the z direction in the geodetic system. From a structural point of view, this test case is clearly within the linear regime. The results show an acceptable agreement of the tip displacements from UM/NAST and the proposed method. Although the amplitudes are significantly different, they are in phase for the first four seconds of the flight (the time of the tail rotation). Also the pitch angle (theta) and the location in the geodetic system (z_g) agree well for the first four seconds, but UM/NAST shows a more

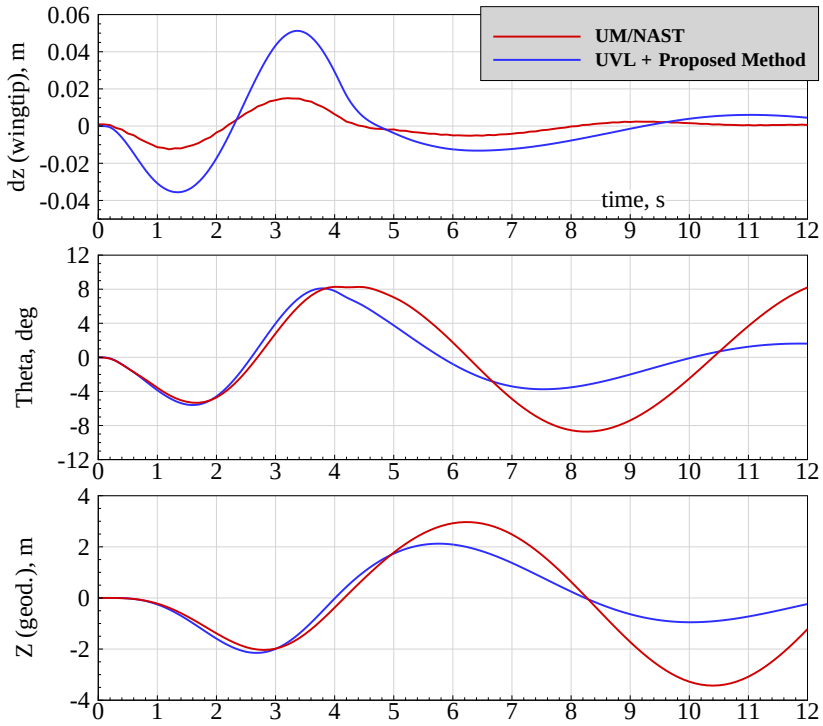

Figure 7: Aircraft response to simultaneous symmetric sinusoidal rotation of all four tails. Amplitude of rotation 1 degree, frequency 0.25 Hz. Steady trim velocity 16 m/s.

distinctive phugoid motion.

For the second test case shown in Fig. 8, the tails are rotated asymmetrically (amplitude of right tails two degrees, left tails one degree). The asymmetric excitation leads to asymmetric structural deflections and rigid body motion around all axes. Similarly to the symmetric case, the deformations of the wing on both sides calculated by UM/NAST are much lower than the deformations from the proposed method, but an acceptable agreement is given for the pitch angle and the location z_g in the geodetic frame. The amplitude of the rigid body motion from UM/NAST is lower compared to the proposed method, and the yaw angle (psi) shows completely different behavior. A possible reason for the differences is that the pods are modeled as slender bodies in UM/NAST whereas they are represented as normal lifting surfaces in the UVL framework. This could result in different sideforces as the aircraft encounters sideslip and rotates around the body frame's z axis.

The next two test cases use a gust disturbance to excite unsteady motion. The *DARPA* gust profile was chosen because it allows varying the disturbance velocity along the span of the aircraft and, by proper choice of its parameters, leads to strong structural excitations with comparatively low rigid body motions as the aircraft passes through the gust. Here, the disturbance velocity of the gust is fixed in the geodetic frame and given as:

$$V_{gust}(X,Y) = \frac{1}{2}U_{ds}\left(1-\cos\left(\frac{2\pi x}{H}\right)\right)\cos\left(\frac{\pi y}{\lambda}-\phi\right) \quad , \tag{44}$$

where U_{ds} was set to 0.5 m/s and 2 m/s respectively for the two test cases presented in the following. The gust length H was set to 40 m, and λ to 3 m.

The first DARPA gust test case (U_{ds} = 0.5 m/s) is presented in Fig. 9. The disturbance of the

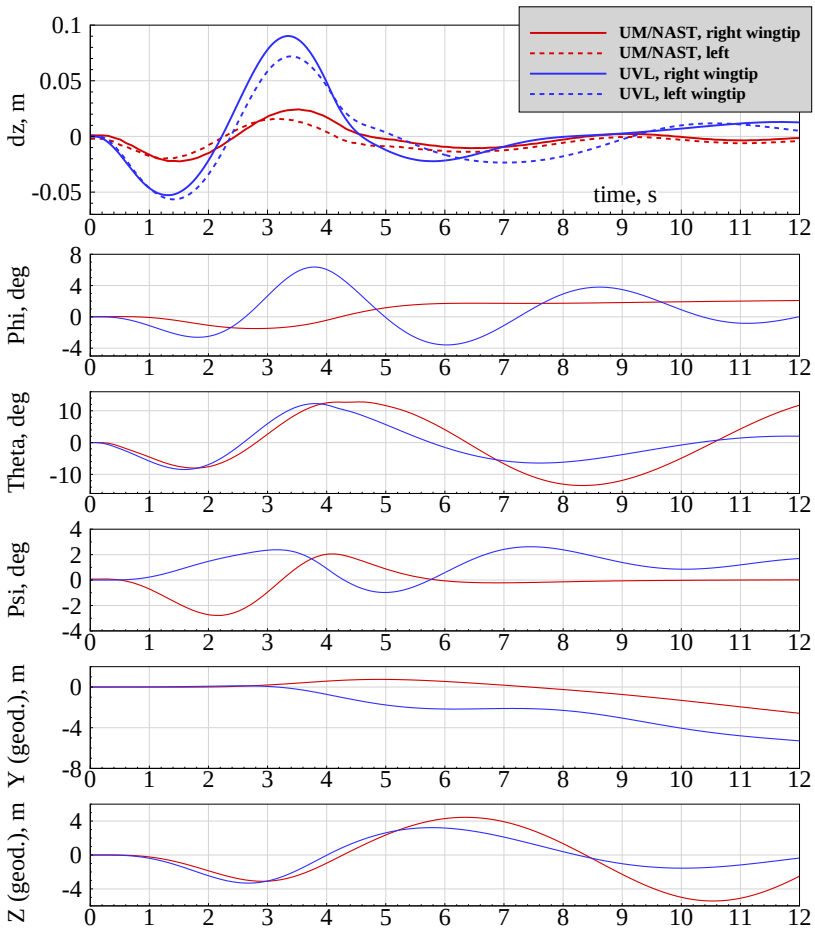

Figure 8: Aircraft response to simultaneous asymmetric sinusoidal rotation of all four tails. Amplitude of rotation 2 and 1 degrees (right and left tails, respectively), frequency 0.25 Hz. Steady trim velocity 16 m/s.

gust leads to a dynamic deflection of the wingtip of approximately 0.22 m, which corresponds, together with the trim deflection of 0.16 m, to a total wing deflection of 12% normalized to the wingspan (3 m). This is slightly beyond the linear structural regime. Both UM/NAST and the proposed method show good agreement in terms of the wingtip deflection. As with the symmetric tail rotation maneuver, the rigid body motion calculated by the aeroelastic framework with the unsteady vortex lattice method are less in amplitude and a significant shift in the phase occurs for both the pitch angle and the location in the z_g direction.

The disturbance velocity was increased to 2 m/s for the second gust case, whose results are shown in Fig. 10. The wing deflections calculated by UM/NAST are higher in this case then the UVL ones, which yields, together with the trim deflection, approximately 30% normalized tip displacement, a highly nonlinear state. The pitch angles agree at a simulation time of two seconds but show larger deviations both in terms of amplitude and phase after that. The location in the geodetic z_g direction are close in amplitude but their temporal relation differs. Snapshots of the X-HALE passing the 2 m/s DARPA gust case are shown in Fig. 11, where the large structural deformations are remarkable.

The question about the differences between the UM/NAST results and the aeroelastic framework with the UVL and the proposed method is not easy to answer. The major difficulty is that the simulation results presented were calculated by completely different aerodynamic and structural dynamic disciplines. The UM/NAST toolbox uses a strip theory to calculate the aero-

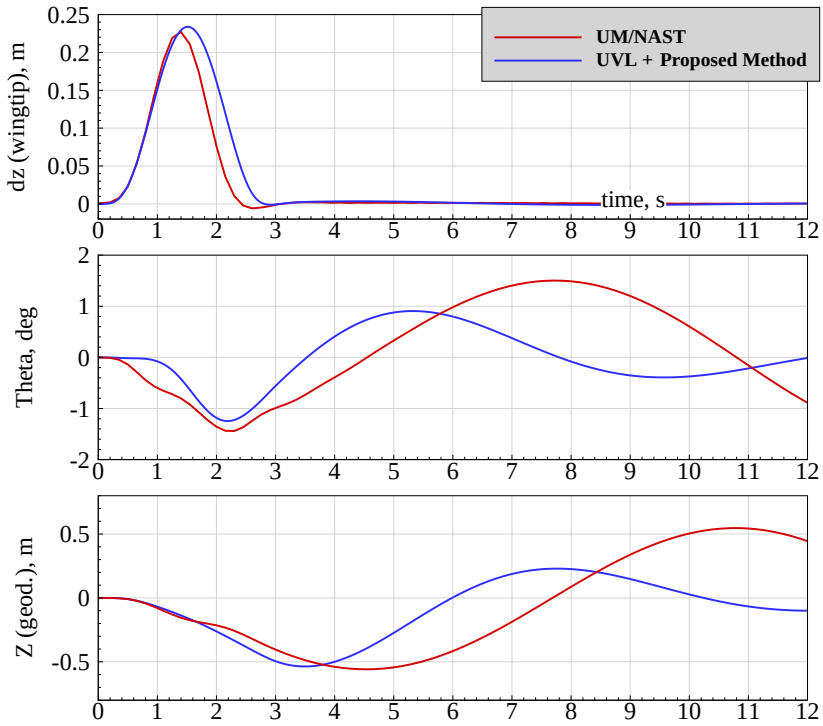

Figure 9: Aircraft response to symmetrical gust disturbance. DARPA gust profile with disturbance velocity of 0.5 m/s. Steady trim velocity 16 m/s.

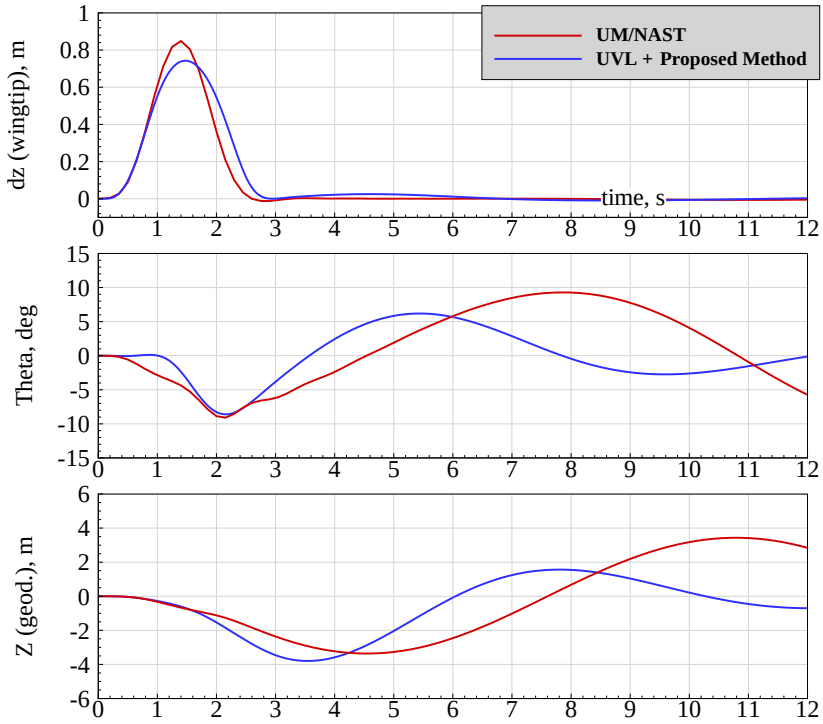

Figure 10: Aircraft response to symmetrical gust disturbance. DARPA gust profile with disturbance velocity of 2 m/s.

dynamic forces, where a time-domain approximation of Theodorsen's function is applied. The simplicity of this method comes with the drawback that the mutual interactions of the aircraft's lifting surfaces is not captured. The X-HALE configuration is especially sensitive in this regard because the lifting surfaces of the pods, tails, and fins can be expected to develop intense

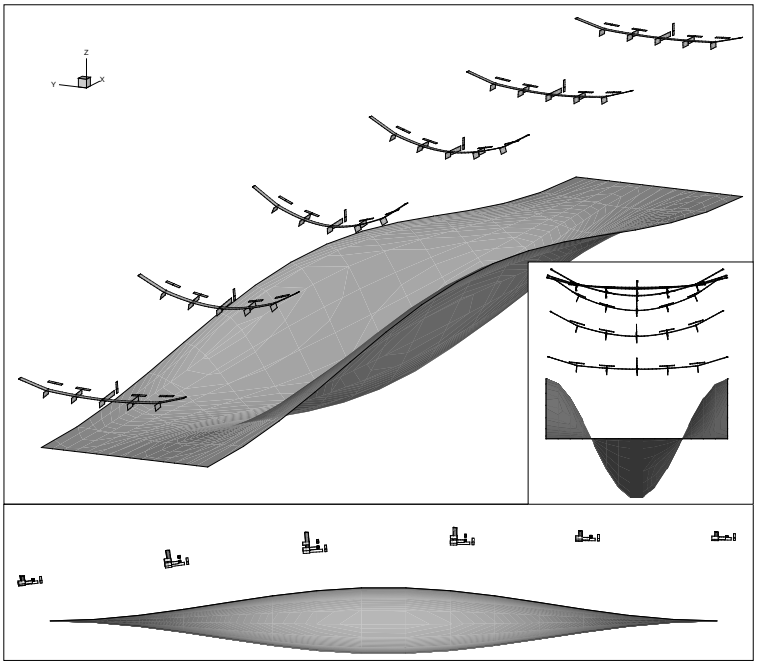

Figure 11: Snapshots of the X-HALE passing the DARPA gust show large wing deformation in the U_{ds} = 2 m/s test case.

aerodynamic interactions. Also the wake of the wing and its interaction with the tails is not modeled. On the other hand, the UM/NAST toolbox uses a very sophisticated, geometrically exact strain-based beam theory. Thus the structural dynamics are expected to be captured in a highly accurate manner. The UVL based framework uses an aerodynamic method that a priori acounts for the interferences of lifting surfaces (and in general captures 3D effects). A better representation of the aerodynamic forces (e.g. lift distribution at the wingtips) is the consequence. Also time dependent effects due to the motion of the wake and the circulation that is shed into the wake leads to different aerodynamic forces, especially on the tails.

6 CONCLUSION

The goal of this work was the application of a framework for the nonlinear aeroelastic simulation of highly flexible aircraft structures to simulate the X-HALE UAV. An extended modal approach that accounts for nonlinear force-displacement relations and a geometrically nonlinear displacement field by the inclusion of higher order stiffness and mode components was extended with rigid body motions. To this end, the flight dynamic governing equations of motion were derived based on Lagrange's equations of the second kind. The higher order stiffness terms are used in the expression of the potential energy, and the calculation of the nodal displacement field uses the higher order mode components. Special emphasis was put on inertial coupling terms between rigid body and elastic motion which leads to a formulation that explicitly avoids the mean-axis constraints. This was done because the higher order mode components can only be calculated for clamped structures. The applied aeroelastic framework is based on an unsteady vortex-lattice method, and a coupling model is used to expand beam-like structural models for the fluid-structure interaction process. Four numerical studies with the X-HALE UAV were presented: Two simple sinusoidal tail excitations that resulted in linear structural deformations, and two gust encounter scenarios where the second one yields nonlinear structural deflections up to 30% normalized tip displacements. Good agreement in terms of structural deflections (both amplitude and phase) were obtained for the gust simulations. The rigid body motions of

UM/NAST and the proposed method, however, are in acceptable agreement only for the first few seconds and show large differences after that. Further numerical studies and validations of the two solvers with the X-HALE UAV are thus indispensable to resolve the differences.

7 REFERENCES

[1] Ritter, M., Cesnik, C. E. S., and Krüger, W. R. (2015). *An Enhanced Modal Approach for Large Deformation Modeling of Wing-Like Structures*. AIAA SciTech. Kissimmee, Florida: 56^{th} AIAA/ASME/ASCE/AHS/ASC Structures, Structural Dynamics, and Materials Conference.

[2] Ritter, M. and Cesnik, C. E. S. (2016). *Large Deformation Modeling of a Beam Type Structure and a 3D Wingbox using an Enhanced Modal Approach*. AIAA SciTech. San Diego, California: 57^{th} AIAA/ASME/ASCE/AHS/ASC Structures, Structural Dynamics, and Materials Conference.

[3] Ritter, M., Jones, J., and Cesnik, C. E. S. (2016). *Enhanced Modal Approach for Free-flight Nonlinear Aeroelastic Simulation of Very Flexible Aircraft*. AIAA SciTech. San Diego, California: 15^{th} Dynamics Specialists Conference.

[4] Cesnik, C. E. S., Palacios, R., and Reichenbach, E. Y. (2014). Reexamined structural design procedures for very flexible aircraft. *Journal of Aircraft*, 51(5).

[5] BUTTRILL, C., ARBUCKLE, P., and ZEILER, T. (1987). *Nonlinear simulation of a flexible aircraft in maneuvering flight*. Guidance, Navigation, and Control and Co-located Conferences. American Institute of Aeronautics and Astronautics.

[6] Meirovitch, L. and Tuzcu, I. (2006). The lure of the mean axes. *Journal of Applied Mechanics*, 74(3), 497–504.

[7] Brockhaus, R. (2013). *Flugregelung*. Springer Berlin Heidelberg. ISBN 9783662072646.

[8] MEIROVITCH, L. (1991). Hybrid state equations of motion for flexible bodies in terms of quasi-coordinates. *Journal of Guidance, Control, and Dynamics*, 14(5), 1008–1013.

[9] Murua, J., Palacios, R., and Graham, J. M. R. (2012). Applications of the unsteady vortex-lattice method in aircraft aeroelasticity and flight dynamics. *Progress in Aerospace Sciences*, 55, 46 – 72.

[10] Katz, J. and Plotkin, A. (2001). *Low-Speed Aerodynamics*. Cambridge Aerospace Series. Cambridge University Press. ISBN 9780521665520.

[11] Ritter, M., Dillinger, J., and Meddaikar, Y. M. (2017). *Static and Dynamic Aeroelastic Validation of a Flexible Forward Swept Composite Wing*. AIAA SciTech Forum. American Institute of Aeronautics and Astronautics.

[12] S. Cesnik, C. E., Senatore, P. J., Su, W., et al. (2012). X-hale: A very flexible unmanned aerial vehicle for nonlinear aeroelastic tests. *AIAA Journal*, 50(12), 2820–2833.

COPYRIGHT STATEMENT